Pergamon

Int. J. Solids Structures Vol. 33, No. 16, pp. 2377–2399, 1996

0020–7683/96 $15.00 + .00

0020–7683(95)00158–1

A MIXED VARIATIONAL FORMULATION FOR INTERLAMINAR STRESSES IN THICKNESS-TAPERED COMPOSITE LAMINATES

PETER N. HARRISON and ERIC R. JOHNSON*
Department of Aerospace and Ocean Engineering, Virginia Polytechnic Institute and State University, Blacksburg, Virginia 24061-0203, U.S.A.

(*Received* 26 *August* 1994; *in revised form* 10 *July* 1995)

Abstract—Stress fields in laminated plates containing an abrupt thickness taper are determined following Pagano's methodology of using the Hellinger-Reissner functional with the stress components approximated within layers by expressions explicit in the thickness coordinate [Pagano, N. J. (1978). Stress fields in composite laminates. *Int. J. Solids Structures* **14**, 385–400; Pagano, N. J. (1983). Axisymmetric stress fields in involute bodies of revolution. In *Advances in Aerospace Structures, Materials and Dynamics*; *A Symposium on Composites, AD-06*, (eds U. Yuceoglu, R. L. Sierakowski and D. A. Glasgow) ASME, NY, pp. 57–64]. The Euler equations from the variational principle are a set of variable coefficient, differential-algebraic equations (DAEs) in the longitudinal coordinate. Difficulties with the number of differential equations and boundary conditions are resolved. Solution of the system is by higher-order one-step finite difference scheme. Numerical ill-conditioning encountered when modeling layers that are thin relative to other layers in a model was remedied by choosing stress shape functions and displacement weighting functions that are different than those used by Pagano. The example problems discussed are dropped-ply laminates (laminates with terminated internal plies), that are subjected to in-plane compression or shear under the assumption that the response is adequately modeled by generalized plane deformation elasticity.

INTRODUCTION

Tapering the thickness of a laminate by terminating, or dropping, internal plies is an important method of stiffness tailoring in structures made from advanced composite materials. Plies are dropped, for example, from root to tip in aircraft wing skins, in composite flexbeams of helicopter rotor hubs, and near field joints in solid rocket boosters. A schematic of a single step asymmetric ply drop-off is shown in Fig. 1. This type of ply drop-off is typically used in applications where a flat surface is important, such as the aforementioned wing skin.

For uniaxial loading normal to the ply termination, experiments and analyses have established that the onset of delamination between the dropped plies and adjacent continuous plies in the vicinity of the ply termination is usually the first major failure event. For example, see the papers by Curry *et al.* (1992), Fish and Lee (1989), and Wisnom (1991, 1992). Consequently, the analyses for the response and failure of dropped-ply laminates have focused on the determination of interlaminar stresses at the ply termination

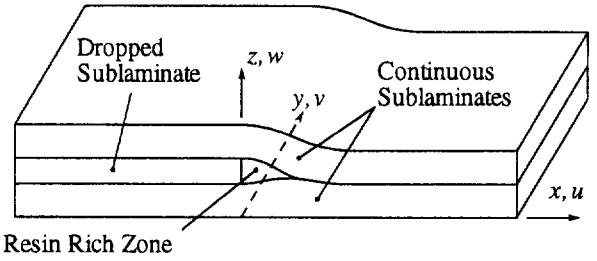

Fig. 1. Tapered laminate with a single step drop.

*Author to whom correspondence should be addressed.

combined with a failure criterion. Criteria for the onset of delamination are either based on interlaminar stresses (Fish and Lee, 1989) or fracture mechanics (Salpekar *et al.* 1988; Wisnom, 1991 and 1992). Most analysts, including those in the references cited here, use the displacement-based finite element method. The best locations for accurate stress computations using this finite element method are at the Gauss points in the interior of the element (Barlow, 1976), and not at the interfaces between adjacent elements. Indeed, interlaminar traction continuity is not guaranteed with the displacement-based finite element method. Since we seek a method of analysis that accurately predicts interlaminar stresses, conditions of traction and displacement continuity between lamina should be satisfied.

Employing the Hellinger-Reissner variational principle, Pagano (1978, 1983) developed a laminate structural theory that satisfied both displacement and traction continuity point-wise at the interface between lamina. For a class of free edge boundary value problems in which dependent variables are functions of one coordinate, this theory led to $13N$ differential-algebraic equations (DAEs) governing the response, where N denotes the number of mathematical layers. Convergence of the theory to the elasticity solution is expected for increasing values of N. Pagano (1978) solved these equations in closed form, but numerical results for $N > 6$ could not be obtained because of computer limitations. Pagano and Whitford (1985) and Pagano (1986) used the theory extended to shells of revolution (Pagano, 1983) to obtained finite difference solutions for the axisymmetric response of a conical frustum under constant temperature change.

Sandhu *et al.* (1991) developed a finite element model of Pagano's (1978) original theory. This theory applies to flat, uniform thickness laminates and results in a system of partial differential equations in the plane of the laminate. The procedure Sandhu *et al.* followed was to develop a self-adjoint version of Pagano's governing equations, which were not self-adjoint as published, from which they derived a new variational formulation and ultimately a two-dimensional finite element model. However, this solution method for the uniform thickness laminates is very involved, and it would increase in complexity if applied to the dropped-ply laminate configuration.

The objective of this paper is to develop a numerical solution for the dropped-ply laminate configuration using Pagano's (1978 and 1983) laminate structural theory. Although this theory (Pagano, 1983) was formulated for curved layers with variable thickness, the solutions presented by Pagano and Whitford (1985) and Pagano (1986) were for layers with straight meridians and uniform thickness. In the development of the numerical solution detailed in this paper, we had to make modifications to shape functions of the original theory to avoid numerical ill conditioning, and to determine a procedure to resolve the number of boundary conditions with the order of the governing DAE system of equations. Numerical results are presented for parametric studies on the effects of load path eccentricity and stiffness change across the taper on delamination initiation.

VARIATIONAL PRINCIPLE

The Hellinger-Reissner variational principle is used to derive compatibility equations consistent with assumed stresses. Consider a body that occupies a volume V, which is subdivided into N subvolumes V_k, with M internal interfaces I_l and with external surface S. The portion of the surface with tractions prescribed is denoted by S_σ while S_u represents the portion with displacements prescribed. Using a cartesian reference with coordinates x_i, $i = 1, 2, 3$, denote the displacements by u_i, strains by ε_{ij}, stresses by σ_{ij}, surface tractions by τ_i and the complementary strain energy density by W^*. The tilde symbol ($\tilde{}$) indicates a prescribed value and repeated indices are summed from one to three in the usual indicial notation. Neglecting body forces, the principle states

$$\sum_{k=1}^{N} \int_{V_k} \left[\left(\frac{u_{i,j} + u_{j,i}}{2} - \frac{\partial W^*}{\partial \sigma_{ij}} \right) \delta\sigma_{ij} - \sigma_{ji,j} \delta u_i \right]^{(k)} \mathrm{d}V_k + \int_{S_\sigma} (\tau_i - \tilde{\tau}_i) \delta u_i \, \mathrm{d}S$$

$$- \int_{S_u} (u_i - \tilde{u}_i) \delta\tau_i \, \mathrm{d}S + \sum_{l=1}^{M} \int_{I_l} [\tau_i^- \delta u_i^- + \tau_i^+ \delta u_i^+] \, \mathrm{d}I_l = 0 \quad (1)$$

in which the comma convention is used to indicate partial differentiation with respect to coordinate x_i. The + and − superscripts denote the two sides of an internal interface. The variational statement of eqn (1), which incorporates the linear strain-displacement relations and symmetry of the stress tensor, is to vanish for every admissible variation in $\delta\sigma_{ij}$ and δu_i.

Admissibility of the stresses and displacements is governed by the boundary conditions and the unique definability of the Hellinger-Reissner functional. For the functional to be uniquely defined, the term $\sigma_{ij}\varepsilon_{ij}$ must be integrable throughout the domain. While there are other possibilities to ensure this, continuity of the displacements throughout the domain is imposed, thereby eliminating the possibility of a delta function in the strains and guaranteeing integrability of the term even when the stresses are not continuous. In addition to this requirement on the displacements, it is desired to develop a theory in which tractions are continuous between layers. In summary, admissible variations in the displacements are to be continuous within subvolumes and at interfaces, and vanish on S_u, and admissible stress variations are symmetric ($\delta\sigma_{ij} = \delta\sigma_{ji}$), continuous in subvolumes, satisfy traction continuity at interfaces, and vanish on S_σ.

For the dropped-ply problem shown in Fig. 1, the more conventional notation of x, y, and z for the coordinates and u, v, and w for the respective displacements are used. In addition, contracted notation is employed for the stresses and engineering strains such that $[\sigma_{xx}, \sigma_{yy}, \sigma_{zz}, \sigma_{yz}, \sigma_{xz}, \sigma_{xy}]^T = [\sigma_1, \sigma_2, \sigma_3, \sigma_4, \sigma_5, \sigma_6]^T$ with the same order for the strains.

GENERALIZED PLANE DEFORMATION

Generalized plane deformation is a class of problems in which the stresses, geometric and material properties, and hence strains are independent of a coordinate direction, in this case y. This assumption differs from generalized plane strain in that it allows bending about the x- and z-axes and twisting about the y-axis. The solution domain is reduced to the x-z plane where the x-axis is the longitudinal axis and the z-axis is the thickness direction (see Fig. 1).

For generalized plane deformation, the most general form of the displacement field is (Lekhnitskii, 1981)

$$\begin{aligned} u(x,y,z) &= -1/2Ay^2 + \theta yz + U(x,z) + u' \\ v(x,y,z) &= (Ax + Bz + C)y + V(x,z) + v' \\ w(x,y,z) &= -1/2By^2 - \theta xy + W(x,z) + w' \end{aligned} \tag{2}$$

where A and B are the negative bending curvatures in the x-y and y-z planes respectively, C is the normal strain ε_y at $x = 0$ and $z = 0$, and the product θy is the rotation of a cross section about the y axis. A, B, C, and θ are all constant over the domain and are the prescribed out-of-plane deformation quantities. The functions U, V and W are the unknown portions of the displacements and u', v' and w' are the rigid body displacements.

DEVELOPMENT OF THE STRUCTURAL MODEL

Assumptions for a generic layer

The subvolumes of the domain take the form of layers, as layers are the most appropriate for the treatment of laminates. These layers may have curved boundaries and need not have uniform thickness. The stress field is approximated within a layer. Consider a generic layer with lower and upper boundaries at $z_1(x)$ and $z_2(x)$ respectively, with z_1 and z_2 smooth functions of x and $z_2 > z_1$ for all x. Following Pagano (1983), the stress field within a typical layer takes the form

$$\sigma_i(x,z) = \sigma_{iJ}(x) f_J^{(i)}(x,z) \quad i = 1 \to 6, J = 1 \to 4 \quad \text{(no sum on } i\text{)}, \tag{3}$$

where σ_i are the six stress components in contracted notation, σ_{iJ} are functions only of x, and $f_j^{(i)}$ are shape functions with explicit dependence on z and known implicit dependence on x through z_1 and z_2. The requirement that $\sigma_{i1} = \sigma_i(z_1)$ and $\sigma_{i2} = \sigma_i(z_2)$ is imposed in order to facilitate interlayer traction continuity.

In arriving at the specific form of the shape functions, the in-plane stresses σ_x, σ_y and σ_{xy} (σ_1, σ_2, and σ_6 in contracted notation) are assumed to have linear dependence on z. Based on the y-independent form of the elasticity equations of equilibrium, the through the thickness distribution of the remaining stress components are determined. The through-the-thickness shear stresses σ_{yz} and σ_{xz} (σ_4 and σ_5) are found to have quadratic dependence on z and the thickness normal stress σ_z (σ_3) has a cubic distribution. The nonzero shape functions are

$$\begin{aligned}
f_1^{(1)} &= f_1^{(2)} = f_1^{(3)} = f_1^{(4)} = f_1^{(5)} = f_1^{(6)} = \frac{z_2 - z}{z_2 - z_1} \\
f_2^{(1)} &= f_2^{(2)} = f_2^{(3)} = f_2^{(4)} = f_2^{(5)} = f_2^{(6)} = \frac{z - z_1}{z_2 - z_1} \\
f_3^{(3)} &= f_3^{(4)} = f_3^{(5)} = \frac{z^2 - z(z_1 + z_2) + z_1 z_2}{(z_2 - z_1)^2} \\
f_4^{(3)} &= \frac{2z^3 - 3z^2(z_1 + z_2) + z(z_1^2 + 4z_1 z_2 + z_2^2) - z_1 z_2 (z_1 + z_2)}{(z_2 - z_1)^3}.
\end{aligned} \tag{4}$$

The last two shape functions are referred to as bubble functions since they are zero at the boundaries of the layer.

The forms of these bubble functions differ from those chosen by Pagano in two ways. First, the cubic bubble function was chosen to be orthogonal to the quadratic one within a layer, i.e. the integral of their product through the layer is zero. This was done in an attempt to overcome conditioning problems when the governing equations were solved numerically. Although this was not sufficient in and of itself to overcome the problem (a different choice of weighting functions, which will be detailed later, solved that problem), it did improve conditioning and provided the added benefit of simplifying the governing equations resulting from application of the variational principle. Second, they are scaled by powers of the thickness $(z_2 - z_1)$ in order to nondimensionalize them and to keep their amplitudes from becoming disproportionately small for thin layers.

The form of W^* for linear-elastic materials in terms of the stresses in contracted notation is

$$W^* = \tfrac{1}{2} S_{ij} \sigma_i \sigma_j, \quad i,j = 1, \ldots, 6 \tag{5}$$

where S_{ij} are the compliance coefficients. This expression is substituted into eqn (1) along with the strain field based on the displacements of eqn (2), the assumed stress field and its variation,

$$\delta\sigma_i(x,z) = \delta\sigma_{iJ}(x) f_J^{(i)}(x,z) \quad \text{(no sum on } i\text{)}, \tag{6}$$

and Cauchy's relation for the tractions in terms of the stresses. Integration with respect to y is carried out through a unit depth, reducing the volume integral to an area integral in the x-z plane and the surface integrals to line integrals. Integration with respect to z is then carried out. Because of the dependence of z_1 and z_2 on x, Leibnitz's theorem must be used on terms involving derivatives in x.

At this point, the displacement terms U, V and W are the only remaining unknowns in the integrand that are functions of z. In order to complete the integration, the following definitions for weighted integrals are made within each layer:

$$[\bar{g}(x), \check{g}(x), \hat{g}(x)] = \int_{z_1}^{z_2} [h_1, h_2, h_3] g(x, z)\, \mathrm{d}z$$

where

$$h_1 = \frac{z_2 - z}{(z_2 - z_1)^2}$$

$$h_2 = \frac{z - z_1}{(z_2 - z_1)^2}$$

$$h_3 = \frac{z^2 - z(z_1 + z_2) + z_1 z_2}{(z_2 - z_1)^3} \tag{7}$$

with g representing a displacement component.

The weighting functions for the displacements in eqn (7) are different from Pagano's, which are simple powers of the thickness coordinate; i.e. 1, z, and z^2. For thin layers or layers located at moderately large values of z relative to the layer thickness, function z^2 is numerically well approximated by a linear combination of 1 and z. The present change in the weighting functions improves the linear independence of the functions, and solved the problem with numerically ill conditioned system matrices.

Layer assembly

A schematic of an assembly of N layers is shown in Fig. 2 along with some notation. The z-coordinate of the kth interface, the top of layer k, is designated $z_k(x)$, and the angle between the horizontal and the tangent to interface k, measured positive counter-clockwise, is γ_k. From the geometry, $z_k'(x) = \tan \gamma_k(x)$, where a prime denotes an ordinary derivative with respect to x. The bottom of layer 1 and the top of layer N are part C^s of the edge curve C, and ends $x = x_1$ and $x = x_1$ $(x_2 > x_1)$ are part C^e of C $(C = C^s + C^e)$.

Layer variables are denoted by the layer number in parentheses as a superscript. Additional subscripts 1 and 2 are used to denote dependent variables evaluated at the bottom and top, respectively, of a layer; e.g. $u^{(k)}(x, z_{k-1}(x)) = u_1^{(k)}(x)$ and $u^{(k)}(x, z_k(x)) = u_2^{(k)}(x)$.

The form of the variational principle arrived at through substituting eqns (2), (3), (5) and (6) into eqn (1), and using definitions given in eqns (4) and (7), is

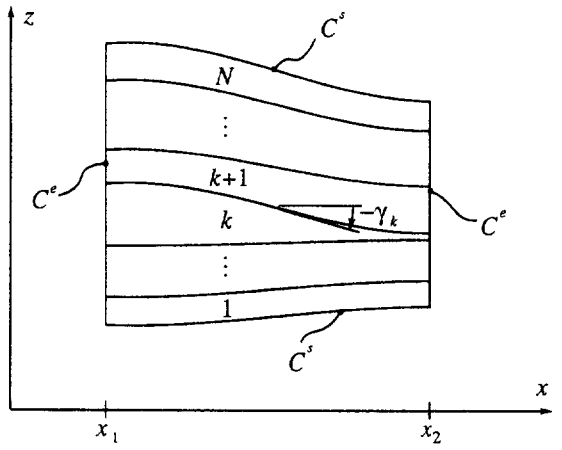

Fig. 2. Schematic of layer assemblage.

$$\int_{x_1}^{x_2}\Bigg\{\sum_{k=1}^{N}[(\mu_{iJ}+\chi_{iJ})^{(k)}\delta\sigma_{iJ}^{(k)}-(G_1\delta\bar{U}+G_2\delta\tilde{U}+G_3\delta\bar{V}+G_4\delta\tilde{V}+G_5\delta\bar{W}+G_6\delta\tilde{W}+G_7\delta\hat{W})^{(k)}]$$

$$+\langle[(\tau_{x1}-\tilde{\tau}_{x1})^{(1)}\delta u_1^{(1)}+(\tau_{y1}-\tilde{\tau}_{y1})^{(1)}\delta v_1^{(1)}+(\tau_{z1}-\tilde{\tau}_{z1})^{(1)}\delta w_1^{(1)}]\sec\gamma_0$$

$$+[(\tau_{x2}-\tilde{\tau}_{x2})^{(N)}\delta u_2^{(N)}+(\tau_{y2}-\tilde{\tau}_{y2})^{(N)}\delta v_2^{(N)}+(\tau_{z2}-\tilde{\tau}_{z2})^{(N)}\delta w_2^{(N)}]\sec\gamma_N\rangle_{C_\sigma^s}$$

$$-\langle[(u_1-\tilde{u}_1)^{(1)}\delta\tau_{x1}^{(1)}+(v_1-\tilde{v}_1)^{(1)}\delta\tau_{y1}^{(1)}+(w_1-\tilde{w}_1)^{(1)}\delta\tau_{z1}^{(1)}]\sec\gamma_0$$

$$+[(u_2-\tilde{u}_2)^{(N)}\delta\tau_{x2}^{(N)}+(v_2-\tilde{v}_2)^{(N)}\delta\tau_{y2}^{(N)}+(w_2-\tilde{w}_2)^{(N)}\delta\tau_{z2}^{(N)}]\sec\gamma_N\rangle_{C_u^s}$$

$$+\sum_{k=1}^{N-1}[(\sigma_{52}^{(k)}-\sigma_{12}^{(k)}z_k')\delta u_2^{(k)}+(\sigma_{11}^{(k+1)}z_k'-\sigma_{51}^{(k+1)})\delta u_1^{(k+1)}+(\sigma_{42}^{(k)}-\sigma_{62}^{(k)}z_k')\delta v_2^{(k)}$$

$$+(\sigma_{61}^{(k+1)}z_k'-\sigma_{41}^{(k+1)})\delta v_1^{(k+1)}+(\sigma_{32}^{(k)}-\sigma_{52}^{(k)}z_k')\delta w_2^{(k)}+(\sigma_{51}^{(k+1)}z_k'-\sigma_{51}^{(k+1)})\delta w_1^{(k+1)}]\Bigg\}\mathrm{d}x$$

$$+\sum_{k=1}^{N}\{\langle[(\sigma_{11}-\tilde{\sigma}_{11})^{(k)}\delta\bar{U}^{(k)}+(\sigma_{12}-\tilde{\sigma}_{12})^{(k)}\delta\tilde{U}^{(k)}+(\sigma_{61}-\tilde{\sigma}_{61})^{(k)}\delta\bar{V}^{(k)}$$

$$+(\sigma_{62}-\tilde{\sigma}_{62})^{(k)}\delta\tilde{V}^{(k)}+(\sigma_{51}-\tilde{\sigma}_{51})^{(k)}\delta\bar{W}^{(k)}+(\sigma_{52}-\tilde{\sigma}_{52})^{(k)}\delta\tilde{W}^{(k)}$$

$$+(\sigma_{53}-\tilde{\sigma}_{53})^{(k)}\delta\hat{W}^{(k)}](z_k-z_{k-1})\rangle_{C_\sigma^c}-\langle[(\bar{U}-\tilde{\bar{U}})^{(k)}\delta\sigma_{11}^{(k)}+(\tilde{U}-\tilde{\tilde{U}})^{(k)}\delta\sigma_{12}^{(k)}$$

$$+(\bar{V}-\tilde{\bar{V}})^{(k)}\delta\sigma_{61}^{(k)}+(\tilde{V}-\tilde{\tilde{V}})^{(k)}\delta\sigma_{62}^{(k)}+(\bar{W}-\tilde{\bar{W}})^{(k)}\delta\sigma_{51}^{(k)}+(\tilde{W}-\tilde{\tilde{W}})^{(k)}\delta\sigma_{52}^{(k)}$$

$$+(\hat{W}-\tilde{\hat{W}})^{(k)}\delta\sigma_{53}^{(k)}](z_k-z_{k-1})\rangle_{C_u^c}\}_{x_1}^{x_2}=0. \tag{8}$$

The integral on x from x_1 to x_2 in this equation contains compatibility equations associated with the sixteen variations $\delta\sigma_{iJ}$, equilibrium equations associated with the seven variations in weighted displacements, traction or displacement prescribed conditions on C^s, and interfacial conditions in which Cauchy's formula was used for the surface tractions. The remaining terms in eqn (8) are boundary terms evaluated on C^e of C.

The compatibility equations in the variational principle (8) have the terms μ_{iJ}, which contain displacements evaluated at the interface, and terms χ_{iJ}, which are displacement-stress relations. The nonzero μ_{iJ} terms are

$$\begin{aligned}
\mu_{11}^{(k)} &= z_{k-1}'u_1^{(k)} & \mu_{12}^{(k)} &= -z_k'u_2^{(k)}\\
\mu_{31}^{(k)} &= -w_1^{(k)} & \mu_{32}^{(k)} &= w_2^{(k)}\\
\mu_{41}^{(k)} &= -v_1^{(k)} & \mu_{42}^{(k)} &= v_2^{(k)}\\
\mu_{51}^{(k)} &= -u_1^{(k)}+z_{k-1}'w_1^{(k)} & \mu_{52}^{(k)} &= u_2^{(k)}-z_k'w_2^{(k)}\\
\mu_{61}^{(k)} &= z_{k-1}'v_1^{(k)} & \mu_{62}^{(k)} &= -z_k'v_2^{(k)}.
\end{aligned} \tag{9}$$

The χ_{iJ} are

$$\chi_{iJ}^{(k)}=\Gamma_{iJ}^{(k)}+\eta_{iJ}^{(k)}-\hat{S}_{ijKJ}^{(k)}\sigma_{jK}^{(k)} \tag{10}$$

in which weighted integrals of the compliances are defined by

$$\hat{S}_{ijKJ}^{(k)}=\int_{z_{k-1}}^{z_k}S_{ij}f_K^{(i)}f_J^{(j)}\,\mathrm{d}z \tag{11}$$

and the out-of-plane prescribed strains are contained in the terms

$$\begin{aligned}
\Gamma_{21}^{(k)} &= 1/6(z_k - z_{k-1})[3(Ax+C) + B(2z_{k-1} + z_k)] \\
\Gamma_{22}^{(k)} &= 1/6(z_k - z_{k-1})[3(Ax+C) + B(z_{k-1} + 2z_k)] \\
\Gamma_{41}^{(k)} &= -1/2(z_k - z_{k-1})\theta x \\
\Gamma_{42}^{(k)} &= -1/2(z_k - z_{k-1})\theta x \\
\Gamma_{43}^{(k)} &= 1/6(z_k - z_{k-1})\theta x \\
\Gamma_{61}^{(k)} &= 1/6(z_k - z_{k-1})(2z_{k-1} + z_k)\theta \\
\Gamma_{62}^{(k)} &= 1/6(z_k - z_{k-1})(z_{k-1} + 2z_k)\theta.
\end{aligned} \tag{12}$$

Finally, the nonzero strain measures in terms of weighted displacement are

$$\begin{aligned}
\eta_{11}^{(k)} &= (z_k - z_{k-1})\bar{U}^{(k)\prime} + (z_k' - 2z_{k-1}')\bar{U}^{(k)} - z_k'\check{U}^{(k)} \\
\eta_{12}^{(k)} &= (z_k - z_{k-1})\check{U}^{(k)\prime} + z_{k-1}'\bar{U}^{(k)} + (2z_k' - z_{k-1}')\check{U}^{(k)} \\
\eta_{31}^{(k)} &= \bar{W}^{(k)} + \check{W}^{(k)} \quad \eta_{32}^{(k)} = -\bar{W}^{(k)} - \check{W}^{(k)} \\
\eta_{33}^{(k)} &= \bar{W}^{(k)} - \check{W}^{(k)} \quad \eta_{34}^{(k)} = -\bar{W}^{(k)} - \check{W}^{(k)} - 6\hat{W}^{(k)} \\
\eta_{41}^{(k)} &= \bar{V}^{(k)} + \check{V}^{(k)} \quad \eta_{42}^{(k)} = -\bar{V}^{(k)} - \check{V}^{(k)} \\
\eta_{43}^{(k)} &= \bar{V}^{(k)} - \check{V}^{(k)} \\
\eta_{51}^{(k)} &= (z_k - z_{k-1})\bar{W}^{(k)\prime} + (z_k' - 2z_{k-1}')\bar{W}^{(k)} - z_k'\check{W}^{(k)} + \bar{U}^{(k)} + \check{U}^{(k)} \\
\eta_{52}^{(k)} &= (z_k - z_{k-1})\check{W}^{(k)\prime} + z_{k-1}'\bar{W}^{(k)} + (2z_k' - z_{k-1}')\check{W}^{(k)} - \bar{U}^{(k)} - \check{U}^{(k)} \\
\eta_{53}^{(k)} &= (z_k - z_{k-1})\hat{W}^{(k)\prime} - z_{k-1}'\bar{W}^{(k)} + z_k'\check{W}^{(k)} + 3(z_k' - z_{k-1}')\hat{W}^{(k)} + \bar{U}^{(k)} - \check{U}^{(k)} \\
\eta_{61}^{(k)} &= (z_k - z_{k-1})\bar{V}^{(k)\prime} + (z_k' - 2z_{k-1}')\bar{V}^{(k)} - z_k'\check{V}^{(k)} \\
\eta_{62}^{(k)} &= (z_k - z_{k-1})\check{V}^{(k)\prime} + z_{k-1}'\bar{V}^{(k)} + (2z_k' - z_{k-1}')\check{V}^{(k)}.
\end{aligned} \tag{13}$$

We impose interfacial continuity conditions on the set of admissible displacements and stresses and their variations. Interlayer continuity of displacements is stated as

$$\begin{aligned}
u_2^{(k)} &= u_1^{(k+1)} \\
v_2^{(k)} &= v_1^{(k+1)} \\
w_2^{(k)} &= w_1^{(k+1)}
\end{aligned} \tag{14}$$

with the same conditions on their variations. Substituting these relationships into the principle combines the six interfacial terms into three traction continuity conditions at each of the internal interfaces:

$$\begin{aligned}
(\sigma_{52}^{(k)} - z_k'\sigma_{12}^{(k)}) &= (\sigma_{51}^{(k+1)} - z_k'\sigma_{11}^{(k+1)}) \\
(\sigma_{42}^{(k)} - z_k'\sigma_{62}^{(k)}) &= (\sigma_{41}^{(k+1)} - z_k'\sigma_{61}^{(k+1)}) \quad k = 1, \ldots, N-1 \\
(\sigma_{32}^{(k)} - z_k'\sigma_{52}^{(k)}) &= (\sigma_{31}^{(k+1)} - z_k'\sigma_{51}^{(k+1)}).
\end{aligned} \tag{15}$$

It is assumed that the variations of the stresses satisfy traction continuity at the interfaces. Substitution of the variations of eqn (15) into the principle combines some of the compatibility terms, reducing their number by $3(N-1)$. Applying the continuity of displacements cancels the μ_{iJ} terms for the internal interfaces, eliminating the interfacial displacements from the formulation. The resulting interfacial compatibility equations are

$$\left.\begin{aligned} \chi_{i2}^{(k)}+\chi_{i1}^{(k+1)}=0;\quad i=1,3,4,5,6 \\ \chi_{12}^{(k)}+z_k'\chi_{52}^{(k)}+(z_k')^2\chi_{32}^{(k)}=0 \\ \chi_{62}^{(k)}+z_k'\chi_{42}^{(k)}=0. \end{aligned}\right\} \quad k=1\rightarrow N-1. \tag{16}$$

Prescribed boundary conditions on the upper and lower surfaces, boundary C^s in Fig. 2, become part of the field equations for the first and Nth layers in the reduction to a two-point boundary value problem. The details are given by Harrison (1994), and the resulting equations are summarized later with the rest of the governing equations.

The equilibrium equations are simply $G_i^{(k)}=0$ where

$$\begin{aligned} G_1^{(k)} &= (z_k-z_{k-1})\sigma_{11}^{(k)\prime}+z_{k-1}'(\sigma_{11}^{(k)}-\sigma_{12}^{(k)})-\sigma_{51}^{(k)}+\sigma_{52}^{(k)}-\sigma_{53}^{(k)} \\ G_2^{(k)} &= (z_k-z_{k-1})\sigma_{12}^{(k)\prime}+z_k'(\sigma_{11}^{(k)}-\sigma_{12}^{(k)})-\sigma_{51}^{(k)}+\sigma_{52}^{(k)}+\sigma_{53}^{(k)} \\ G_3^{(k)} &= (z_k-z_{k-1})\sigma_{61}^{(k)\prime}-\sigma_{41}^{(k)}+\sigma_{42}^{(k)}-\sigma_{43}^{(k)}+z_{k-1}'(\sigma_{61}^{(k)}-\sigma_{62}^{(k)}) \\ G_4^{(k)} &= (z_k-z_{k-1})\sigma_{62}^{(k)\prime}-\sigma_{41}^{(k)}+\sigma_{42}^{(k)}+\sigma_{43}^{(k)}+z_k'(\sigma_{61}^{(k)}-\sigma_{62}^{(k)}) \\ G_5^{(k)} &= (z_k-z_{k-1})\sigma_{51}^{(k)\prime}-\sigma_{31}^{(k)}+\sigma_{32}^{(k)}-\sigma_{33}^{(k)}+\sigma_{34}^{(k)}+z_{k-1}'(\sigma_{51}^{(k)}-\sigma_{52}^{(k)}+\sigma_{53}^{(k)}) \\ G_6^{(k)} &= (z_k-z_{k-1})\sigma_{52}^{(k)\prime}-\sigma_{31}^{(k)}+\sigma_{32}^{(k)}+\sigma_{33}^{(k)}+\sigma_{34}^{(k)}+z_k'(\sigma_{51}^{(k)}-\sigma_{52}^{(k)}-\sigma_{53}^{(k)}) \\ G_7^{(k)} &= (z_k-z_{k-1})\sigma_{53}^{(k)\prime}+6\sigma_{34}^{(k)}-2(z_k'-z_{k-1}')\sigma_{53}^{(k)}. \end{aligned} \tag{17}$$

The remaining equations are layer compatibility equations which are defined for all N layers:

$$\chi_{21}^{(k)}=\chi_{22}^{(k)}=\chi_{33}^{(k)}=\chi_{34}^{(k)}=\chi_{43}^{(k)}=\chi_{53}^{(k)}=0. \tag{18}$$

Resolving the order of the system

The group of equations resulting from this derivation is called a system of differential-algebraic equations (DAEs) because it is composed of both differential and algebraic equations. Solution of such systems can introduce problems in the interpretation of the order of the system, which is not straight-forward.

As presented in eqn (8), the principle contains 29 variables per layer (sixteen stress quantities, seven weighted displacements and three displacements at the bottom and top of the layer) giving a total of $29N$ for a model. There are also $29N$ terms in the integral, composed of a varied quantity and its associated equation. Of these equations, $14N$ are differential, composed of all $7N$ of the equilibrium and $7N$ of the compatibility terms. There are also $7N$ boundary terms at each end. For our case in which the internal layer interfaces are perfectly joined, the number of variables is reduced by $6(N-1)$ with the elimination of internal interfacial displacements (three for each of the two adjacent layer surfaces comprising the interface, of which there are $N-1$). At the same time, the number of terms in the principle is reduced by $6(N-1)$; $3(N-1)$ from combining the interlayer traction terms associated with the variations of the internal interfacial displacements, and $3(N-1)$ from combining layer compatibility terms associated with the variations in the stress components evaluated at the interface. In this procedure, the number of *differential* compatibility equations is reduced by $N-1$ through the combining of layer compatibility terms associated with $\delta\sigma_{12}$ and $\delta\sigma_{52}$. Prescription of the x-direction traction on a surface also reduces the number of differential equations by one.

Thus, after invoking interfacial continuity and surface conditions the system has $23N$ equations and unknowns with $7N$ differential equations of equilibrium, either $6N-1$, $6N$, or $6N+1$ differential equations of compatibility (depending on the surface conditions), and the remaining equations algebraic. In this form, difficulties arise in solving the system having to do with the number of differential equations and boundary conditions. Because the number of differential compatibility equations are reduced without a like reduction in the number of differential equilibrium equations, it is possible to have a system with an odd number of differential equations. Application of the same boundary conditions at each end, giving an even number of boundary conditions, appears to be in conflict with this. This inconsistency was remedied by Pagano (1983) through an involved interpretation of what he calls end conditions. He arrived at these end conditions by assuming the integrand of the functional vanishes at the ends. These conditions were then incorporated into his central difference approximation using three-point forward and backward differences at the ends.

As an alternative to Pagano's interpretation, we use a manipulation of the differential equilibrium equations to reduce their number by the same amount as the differential compatibility. This was done by differentiating the first equation of eqn (15), eliminating $\sigma_{12}^{(k)\prime}, \sigma_{51}^{(k)\prime}$ and $\sigma_{11}^{(k)\prime}$ by substituting from $G_2^{(k)}, G_5^{(k+1)}$, and $G_1^{(k+1)}$, and then substituting this result into $G_6^{(k)}$. (It is worth noting that the traction continuity equation that is differentiated here to eliminate $\sigma_{52}^{(k)\prime}$ is the same one that combined two of the differential compatibility terms when its variation was substituted into the principle.) The new form of the equation is labeled $\hat{G}_6^{(k)}$ and is given by

$$\hat{G}_6^{(k)} = -(z_k')^2\sigma_{11}^{(k)} + [(z_k - z_{k-1})z_k'' + (z_k')^2]\sigma_{12}^{(k)} - \sigma_{31}^{(k)} + \sigma_{32}^{(k)} + \sigma_{33}^{(k)} + \sigma_{34}^{(k)}$$
$$+ 2z_k'(\sigma_{51}^{(k)} - \sigma_{52}^{(k)} - \sigma_{53}^{(k)}) + \frac{(z_k - z_{k-1})}{(z_{k+1} - z_k)}\{[(z_k')^2 - (z_{k-1} - z_k)z_k'']\sigma_{11}^{(k+1)}$$
$$-(z_k')^2\sigma_{12}^{(k+1)} + \sigma_{31}^{(k+1)} - \sigma_{32}^{(k+1)} + \sigma_{33}^{(k+1)} - \sigma_{34}^{(k+1)} + 2z_k'(-\sigma_{51}^{(k+1)} + \sigma_{52}^{(k+1)} - \sigma_{53}^{(k+1)})\}. \quad (19)$$

This equation is defined for $k = 1 \rightarrow N-1$.

The x-direction surface conditions require a similar treatment in order to avoid an odd number of differential equations. The details of the derivation of $\hat{G}_6^{(k)}, \bar{G}_6^{(N)}$, and $\bar{G}_5^{(1)}$ are presented in the dissertation (Harrison, 1994).

Effective compliances for sublaminates

Direct evaluation of the effective compliances given by eqn (11) for mathematical layers comprising multiple plies of varying orientation, or sublaminates, results in an excessively flexible response. Effective compliances that are too large are caused by the assumption of continuous in-plane stresses across the interface of adjacent lamina which, in turn, implies the in-plane strains jump across the interface because of the step change in material properties. Thus, direct application of eqn (11) for sublaminates implies that displacement continuity along the interface between lamina is violated.

To remedy the situation described above, eqn (11) was evaluated for sublaminates by first using a homogenization procedure to determine spatially uniform, three-dimensional effective compliances within the sublaminate. Thus, the compliances in the integrand of eqn (11) are independent of coordinate z for the homogeneous equivalent sublaminate and are factored out. The homogenization scheme employs a combination of the Voigt and Reuss approximations in equating the strain energy of the sublaminate per unit reference surface area to the strain energy per unit reference surface area of a homogeneous equivalent material (Harrison, 1994). The Voigt approximation assumes equivalent strains for differing materials making up a composite and was applied to the in-plane strains. The Reuss approximation assumes equivalent stresses and was applied to the out-of-plane stresses.

GOVERNING EQUATIONS

The governing equations are summarized below with the differential equations underscored and the algebraic equations not underscored.

Compatibility equations

$$\chi_{21}^{(k)} = \chi_{22}^{(k)} = \chi_{33}^{(k)} = \chi_{34}^{(k)} = \chi_{43}^{(k)} = \underline{\chi_{53}^{(k)}} = 0 \quad k = 1 \to N \tag{20}$$

$$\left.\begin{aligned} \chi_{i2}^{(k)} + \chi_{i1}^{(k+1)} &= 0; \qquad i = \underline{1}, 3, 4, \underline{5}, \underline{6} \\ \underline{\chi_{12}^{(k)} + z_k' \chi_{52}^{(k)} + (z_k')^2 \chi_{32}^{(k)}} &= 0 \\ \underline{\chi_{62}^{(k)} + z_k' \chi_{42}^{(k)}} &= 0 \end{aligned}\right\} \quad k = 1 \to N-1 \tag{21}$$

$$\begin{aligned} \underline{\chi_{11}^{(1)} + z_0' \chi_{51}^{(1)} + (z_0')^2 \chi_{31}^{(1)}} &= 0 \\ \underline{\chi_{61}^{(1)} + z_0' \chi_{41}^{(1)}} &= 0 \\ \underline{\chi_{12}^{(N)} + z_N' \chi_{52}^{(N)} + (z_N')^2 \chi_{32}^{(N)}} &= 0 \\ \underline{\chi_{62}^{(N)} + z_N' \chi_{42}^{(N)}} &= 0. \end{aligned} \tag{22}$$

Equilibrium equations

$$\underline{G_1^{(k)}} = \underline{G_2^{(k)}} = \underline{G_3^{(k)}} = \underline{G_4^{(k)}} = \underline{G_7^{(k)}} = 0 \quad k = 1 \to N \tag{23}$$

$$\left.\begin{aligned} \hat{G}_6^{(k)} &= 0 \\ G_5^{(k+1)} &= 0 \end{aligned}\right\} \quad k = 1 \to N-1 \tag{24}$$

with either, for $u_1^{(1)}$ prescribed,

$$\underline{G_5^{(1)}} = 0 \tag{25}$$

or, for $\tau_{x1}^{(1)}$ prescribed,

$$\bar{G}_5^{(1)} = 0 \tag{26}$$

as well as either, for $u_2^{(N)}$ prescribed,

$$\underline{G_6^{(N)}} = 0 \tag{27}$$

or, for $\tau_{x2}^{(N)}$ prescribed,

$$\bar{G}_6^{(N)} = 0. \tag{28}$$

Interlayer traction continuity equations

$$\left.\begin{aligned} (\sigma_{52}^{(k)} - z_k' \sigma_{12}^{(k)}) &= (\sigma_{51}^{(k+1)} - z_k' \sigma_{11}^{(k+1)}) \\ (\sigma_{42}^{(k)} - z_k' \sigma_{62}^{(k)}) &= (\sigma_{41}^{(k+1)} - z_k' \sigma_{61}^{(k+1)}) \\ (\sigma_{32}^{(k)} - z_k' \sigma_{52}^{(k)}) &= (\sigma_{31}^{(k+1)} - z_k' \sigma_{51}^{(k+1)}). \end{aligned}\right\} \quad k = 1 \to N-1 \tag{29}$$

Surface conditions

For layer 1,

$$\underline{\chi_{51}^{(1)} + z_0' \chi_{31}^{(1)} - \tilde{u}_1^{(1)}} = 0 \quad \text{or} \quad \sigma_{11}^{(1)} \sin\gamma_0 - \sigma_{51}^{(1)} \cos\gamma_0 = \tilde{\tau}_{x1}^{(1)} \tag{30}$$

$$\chi_{41}^{(1)} - \tilde{v}_1^{(1)} = 0 \quad \text{or} \quad \sigma_{61}^{(1)} \sin\gamma_0 - \sigma_{41}^{(1)} \cos\gamma_0 = \tilde{\tau}_{y1}^{(1)} \tag{31}$$

$$\chi_{31}^{(1)} - \tilde{w}_1^{(1)} = 0 \quad \text{or} \quad \sigma_{51}^{(1)} \sin\gamma_0 - \sigma_{31}^{(1)} \cos\gamma_0 = \tilde{\tau}_{z1}^{(1)} \tag{32}$$

and for layer N,

$$\underline{\chi_{52}^{(N)} + z'_N \chi_{32}^{(N)} + \tilde{u}_2^{(N)}} = 0 \quad \text{or} \quad \sigma_{52}^{(N)} \cos\gamma_N - \sigma_{12}^{(N)} \sin\gamma_N = \tilde{\tau}_{x2}^{(N)} \tag{33}$$

$$\chi_{42}^{(N)} + \tilde{v}_2^{(N)} = 0 \quad \text{or} \quad \sigma_{42}^{(N)} \cos\gamma_N - \sigma_{62}^{(N)} \sin\gamma_N = \tilde{\tau}_{y2}^{(N)} \tag{34}$$

$$\chi_{32}^{(N)} + \tilde{w}_2^{(N)} = 0 \quad \text{or} \quad \sigma_{32}^{(N)} \cos\gamma_N - \sigma_{52}^{(N)} \sin\gamma_N = \tilde{\tau}_{z2}^{(N)}. \tag{35}$$

Boundary conditions

The boundary conditions are affected by the imposition of traction continuity as well as by the surface conditions. In eqn (8), there are $14N$ boundary terms at the x = constant edges (C^e) of which $7N$ apply depending upon whether displacements or tractions are prescribed. Assuming eqn (15) holds at the end points, substitution of the variational form of the first part of eqn (15) reduces the number of displacement prescription equations by $N-1$. Applying the unvaried form of the same equation reduces the number of independently specifiable stress variables in the traction prescription terms by $N-1$. In a similar manner, for each x-direction surface (C^s) traction prescribed, the number of boundary conditions is reduced by one.

A further point needs to be made regarding the development of the boundary conditions. In order to allow the three tractions to be applied independently, restrictions must be placed on the geometry of the domain at the ends. Specifically, the slope of all layer interfaces is restricted to zero at the ends. The resulting boundary conditions are

$$\left.\begin{aligned} \bar{U}^{(k)} = \tilde{\bar{U}}^{(k)} \text{ and } \check{U}^{(k)} = \tilde{\check{U}}^{(k)} \\ \text{or} \\ \sigma_{11}^{(k)} = \tilde{\sigma}_{11}^{(k)} \text{ and } \sigma_{12}^{(k)} = \tilde{\sigma}_{12}^{(k)} \end{aligned}\right\} \quad k = 1 \to N \tag{36}$$

$$\left.\begin{aligned} \bar{V}^{(k)} = \tilde{\bar{V}}^{(k)} \text{ and } \check{V}^{(k)} = \tilde{\check{V}}^{(k)} \\ \text{or} \\ \sigma_{61}^{(k)} = \tilde{\sigma}_{61}^{(k)} \text{ and } \sigma_{62}^{(k)} = \tilde{\sigma}_{62}^{(k)} \end{aligned}\right\} \quad k = 1 \to N \tag{37}$$

$$\left.\begin{aligned} &(z_k - z_{k-1})\bar{W}^{(k)} + (z_{k+1} - z_k)\bar{W}^{(k+1)} \\ &= (z_k - z_{k-1})\tilde{\bar{W}}^{(k)} + (z_{k+1} - z_k)\tilde{\bar{W}}^{(k+1)} \quad k = 1 \to N-1 \\ &\text{and} \\ &\hat{W}^{(k)} = \tilde{\hat{W}}^{(k)} \qquad\qquad k = 1 \to N \end{aligned}\right\} \tag{38}$$

or

$$\left.\begin{aligned} &\sigma_{51}^{(k+1)} = \tilde{\sigma}_{51}^{(k+1)} \quad k = 1 \to N-1 \\ &\qquad \text{and} \\ &\sigma_{53}^{(k)} = \tilde{\sigma}_{53}^{(k)} \qquad k = 1 \to N \end{aligned}\right.$$

With, for $u_1^{(1)}$ prescribed,

$$\bar{W}^{(1)} = \tilde{\bar{W}}^{(1)} \quad \text{or} \quad \sigma_{51}^{(1)} = \tilde{\sigma}_{51}^{(1)} \tag{39}$$

and for $u_2^{(N)}$ prescribed,

$$\check{W}^{(N)} = \tilde{\check{W}}^{(N)} \quad \text{or} \quad \sigma_{52}^{(N)} = \tilde{\sigma}_{52}^{(N)}. \tag{40}$$

Segment continuity

In order to analyze a dropped-ply laminate, the formulation must also allow step changes in material properties in the longitudinal direction. To accomplish this, the domain is divided into segments, each having its own properties. The solutions for the different segments are then joined through inter-segment continuity conditions. In deriving these conditions, restrictions on the geometry of the adjoining segments must be imposed. Specifically, the layer boundaries must be continuous and the slope of the layer boundaries must also be continuous. The first restriction is required to preserve consistency of definition of the weighted displacements between segments and to allow pointwise traction continuity. The second restriction is imposed because, without it, σ_1, σ_3 and σ_5 would all have to be equal across both the layer and segment interfaces at the junction. The resulting conditions between segments designated a and b are

$$\left.\begin{aligned}
&\sigma_{61a}^{(k)} = \sigma_{61b}^{(k)} \\
&\sigma_{62a}^{(k)} = \sigma_{62b}^{(k)} \\
&\sigma_{53a}^{(k)} = \sigma_{53b}^{(k)} \\
&\sigma_{11a}^{(k)} = \sigma_{11b}^{(k)} \\
&\sigma_{12a}^{(k)} = \sigma_{12b}^{(k)} \\
&\bar{V}_a^{(k)} = \bar{V}_b^{(k)} \\
&\check{V}_a^{(k)} = \check{V}_b^{(k)} \\
&\hat{W}_a^{(k)} = \hat{W}_a^{(k)} \\
&\bar{U}_a^{(k)} + z'_{k-1}\bar{W}_a^{(k)} = \bar{U}_b^{(k)} + z'_{k-1}\bar{W}_b^{(k)} \\
&\check{U}_a^{(k)} + z'_k\check{W}_a^{(k)} = \check{U}_b^{(k)} + z'_k\check{W}_b^{(k)}
\end{aligned}\right\} \quad k = 1 \to N \tag{41}$$

$$\left.\begin{aligned}
&\sigma_{51a}^{(k+1)} = \sigma_{51b}^{(k+1)} \\
&(z_{k+1} - z_k)\bar{W}_a^{(k+1)} + (z_k - z_{k-1})\check{W}_a^{(k)} \\
&= (z_{k+1} - z_k)\bar{W}_b^{(k+1)} + (z_k - z_{k-1})\check{W}_b^{(k)}
\end{aligned}\right\} \quad k = 1 \to N-1 \tag{42}$$

with, for $u_1^{(1)}$ prescribed,

$$\sigma_{51a}^{(1)} = \sigma_{51b}^{(1)} \quad \text{and} \quad \bar{W}_a^{(1)} = \bar{W}_b^{(1)} \tag{43}$$

and for $u_2^{(N)}$ prescribed,

$$\sigma_{52a}^{(N)} = \sigma_{52b}^{(N)} \quad \text{and} \quad \check{W}_a^{(N)} = \check{W}_b^{(N)}. \tag{44}$$

Model summary

Determining the response for a particular problem involves the determination of $23N$ unknowns ($16N$ stress variables and $7N$ weighted displacements) where N is the number of layers. They are determined through the solution of eqns (20) through (35) subject to the boundary conditions of eqns (36) through (40) with the conditions of eqns (41) through (44) between segments of the domain.

NUMERICAL SOLUTION OF THE BOUNDARY VALUE PROBLEM

Due to the curved geometry at the ply drop-off, the first order system has variable coefficients. Written in matrix form, the system is expressed as

$$\mathbf{A}(x)\mathbf{y}'(x)+\mathbf{B}(x)\mathbf{y}(x) = \mathbf{f}(x) \tag{45}$$

where $\mathbf{A}(x)$ is singular due to the algebraic character of some of the equations. This mathematical formulation is classified as a semi-implicit boundary-value DAE system and is a subject of contemporary research (Schiesser, 1994). The solution vector $\mathbf{y}$ for an N-layer problem has the form

$$\mathbf{y}^T = [\mathbf{y}^{(1)^T}, \mathbf{y}^{(2)^T}, \ldots, \mathbf{y}^{(N)^T}] \tag{46}$$

where each $\mathbf{y}^{(k)}$ contains 23 unknowns composed of the 16 stress variables and 7 weighted displacements.

The resulting system is solved using a one-step finite difference approximation. One-step differences were chosen over two-step methods, such as the central, forward, and backward differences used by Pagano *et al.* (1985, 1986), because of their flexibility in handling non-uniform grid spacing as well as their straightforward application at the boundaries for first order systems.

The trapezoidal finite difference scheme was attempted first. However, its accuracy (order 2) was not sufficient, resulting in erroneous results in regions of thickness taper. These errors were further magnified if rigid body displacements were present. The two-stage Gauss implicit Runge-Kutta scheme (order 4) provided the accuracy needed to overcome these errors and is the scheme used for the results given in this paper (see Ascher *et al.* 1988). However, the derivation of this scheme presented in the above reference applies only to fully differential systems. The present system was therefore converted by differentiating the algebraic equations and applying them in their original form as initial conditions. Because the higher order Runge-Kutta scheme involves matrix inversion in arriving at the difference equations for each step, this fully differential system increased the computational expense to achieve improved accuracy over the trapezoidal scheme.

ACCURACY OF THE MODEL

Comparisons of the results obtained with the present model and solution strategy with those published by Pagano (1978) for the benchmark problem of the interlaminar stress response near the straight free edge of a tensile coupon were published earlier (Harrison and Johnson, 1993). These results showed very good agreement, which was expected because the stress assumptions of the present model essentially reduce to Pagano's for uniform thickness flat layers. In addition, we presented a comparison with the displacement based finite element results of Curry *et al.* (1992) for the interlaminar stress response of a dropped-ply laminate subjected to axial compression. The interlaminar stresses were compared along contours passing through the finite element Gauss points, as that is the location of the most accurate values from the finite element analysis. Good agreement was found between the two analyses.

PARAMETRIC STUDIES

The results presented here are for parametric studies of dropped-ply laminates in which the influence of the load path eccentricity and the magnitude of the stiffness discontinuity are examined.

Eccentricity study

When a laminated plate contains an asymmetric ply drop-off, the middle surface is not a plane but instead contains an offset at the drop-off. This eccentricity in the middle surface and the bending moment that is induced would appear to be a factor in the strength

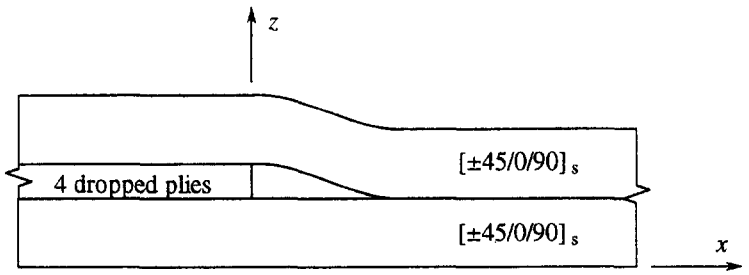

(a) With eccentricity.

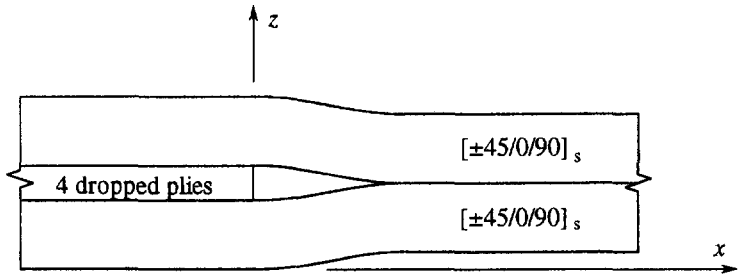

(b) Without eccentricity.

Fig. 3. Laminates with and without eccentricity in the middle surface.

degradation in a dropped-ply laminate. This parametric study was done to determine the effect of eccentricity on the interlaminar stresses present at a ply drop-off.

Two dropped-ply configurations are compared, one that is asymmetric and therefore has an eccentric middle surface, and the other that is symmetric, i.e. no eccentricity (see Fig. 3). These two geometries were examined with three different layups for the dropped plies and under three different loadings for a total of eighteen cases.

In both geometries, the two continuous sublaminates have the same eight ply quasi-isotropic $[\pm 45/0/90]_s$ layup. The dropped sublaminate contains four plies with the layups $[0_4]_T$, $[90_4]_T$, or $[\pm 45]_s$. Each ply has thickness 0.1395 mm (0.0055 in) giving thicknesses 0.558 mm (0.022 in) for the dropped plies, 2.794 mm (0.110 in) for the thick portion, and 2.248 mm (0.0885 in) for the thin. The thin portion also contains a 0.0127 mm (0.0005 in) thick layer of resin between the continuous sublaminates which is a continuation of the layers modeling the resin region and the dropped plies, and is required in order to retain a constant number of layers in the mathematical model throughout the domain. The eccentricity is, therefore, either zero or 0.273 mm (two ply thicknesses minus half the resin layer thickness). The lengths of the thick and thin portions is 25.4 mm (1.0 in) for each and the tapered section is 2.24 mm (0.088 in) long for a total laminate length of 53.04 mm (2.088 in). The origin of the coordinate system for the study is located at the end of the dropped plies, i.e. the beginning of the thickness taper (see Fig. 3).

The model used in this analysis consists of six mathematical layers. That is, in moving from one surface to the other of the thick section, the layers are $[\pm 45/0/90_2/0]$, $[\mp 45]$, $[\pm\theta]$, $[\mp\theta]$, $[\pm 45]$, and $[0/90_2/0/\mp 45]$. With the exception of the 90° cases, the center two layers are modeled as resin from the drop-off, through the transition region, and into the thin section. Experience in manufacturing specimens with 90° dropped plies has shown that these fibers tend to migrate into the area occupied by resin in the $[0_4]_T$ and $[\pm 45]_s$ dropped-ply laminates. For the 90° cases, the triangular shaped resin region is modeled as 90° material with the origin remaining at the thick end of the taper.

The material properties for the individual plies are those of AS4/3502 graphite/epoxy:

$$E_{11} = 128\,\text{GPa} \quad (18.5\,\text{Msi}), \quad E_{22} = E_{33} = 11.3\,\text{GPa} \quad (1.64\,\text{Msi})$$

$$G_{12} = G_{13} = 6.0\,\text{GPa} \quad (0.87\,\text{Msi}), \quad G_{23} = 3.38\,\text{GPa} \quad (0.49\,\text{Msi})$$

$$\nu_{12} = \nu_{13} = 0.3, \quad \nu_{23} = 0.35$$

and for the neat resin:

$$E = 3.45\,\text{GPa} \quad (0.5\,\text{Msi})$$
$$\nu = 0.41.$$

The three load cases are longitudinal compression (along the x-axis), transverse tension (along the y-axis), and shear in the x-y plane. The surfaces of the laminates (C^s in Fig. 2) are considered to be traction-free in all three load cases. The boundary conditions at the left (thick) end ($x = -25.4$ mm) are also the same in all three load cases, with $u = 0$, $v = 0$, and $\tau_z = 0$. Each laminate is constrained from rigid body translation in the z-direction through the prescription of $w = 0$ at the lower surface of a very short (0.254 mm) segment at the left end. The other rigid body modes are excluded through the displacement boundary conditions. The longitudinal compression and in-plane shear loads are applied through prescription of N_x and N_{xy} at the right end ($x = 27.64$ mm), while restraining the u and v displacements, respectively, to uniform values through the thickness. The transverse tension load is applied through prescription of the uniform strain ε_y by taking $A = B = \theta = 0$ and $C = 0.001$ in eqn (2).

Since the primary focus of this study is the effect of eccentricity on the tendency of laminates with dropped plies to delaminate, a measure of this tendency is necessary. Rather than looking at each interlaminar stress component separately, it is desirable to have an index that accounts for the combined effect of the different components. An index similar to the Quadratic Delamination Criterion proposed by Brewer and Lagace (1988) was chosen. This delamination index is defined as

$$F = \left(\frac{\sigma_{tn}}{Z^{S1}}\right)^2 + \left(\frac{\sigma_{yn}}{Z^{S2}}\right)^2 + \left(\frac{\sigma_{nn}}{Z^{T}}\right)^2 \tag{47}$$

in which σ_{nn} denotes the interlaminar normal stress, and σ_{yn} and σ_{tn} denote interlaminar shear stress components, and where Z^{S1}, Z^{S2}, and Z^T are the allowable interlaminar stresses. For AS4/3502, those allowable are assumed to be

$$Z^{S1} = Z^{S2} = 93.08\,\text{MPa}\,(13.5\,\text{ksi})$$
$$Z^{T} = 51.99\,\text{MPa}\,(7.54\,\text{ksi}).$$

The onset of delamination is likely to occur when $F \geqslant 1$. Since index F depends quadratically on the stresses, it is the square root of F which would be directly proportional to the load in the case of proportional loading. Therefore, the distribution of $\sqrt{F}$, referred to as the delamination fraction, will be examined. It should be noted that using eqn (47) with $F = 1$ as a delamination initiation criterion is not meaningful, since the peel stress, or tensile interlaminar normal stress, at the ply termination is likely to be singular in an elasticity solution. This singularity is manifested in our approximate solution by non-convergence of the maximum peel stress as the number of mathematical layers in the model increases. However, eqn (47) with $F = 1$ is used as the basis of a failure criterion if stresses are averaged over the interface or if they are evaluated at some distance from the ply termination.

The delamination fraction was examined along the two critical interfaces, i.e. the top of the lower continuous sublaminate and the bottom of the upper continuous sublaminate. These two interfaces will be referred to as the lower and upper interfaces respectively. For the centric geometry, the distribution of $\sqrt{F}$ is the same for the two interfaces due to symmetry.

Results for the four 0° dropped-ply layup and a longitudinal compression load of $N_x = -1$ kN/m are presented here, with summaries for the other cases presented later. The

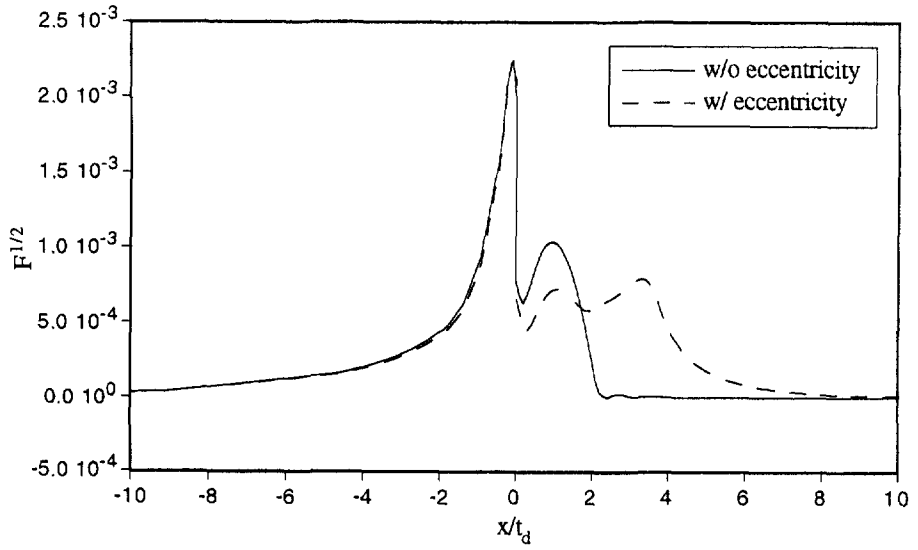

Fig. 4. Delamination fraction along the lower interface for four 0° plies dropped and the laminate loaded in longitudinal compression ($N_x = -1$ kN/m).

delamination fraction for the lower and upper interfaces is plotted vs the normalized longitudinal coordinate x/t_d, where t_d denotes the thickness of the dropped plies, in Figs 4 and 5 respectively. As shown in these figures the eccentricity has essentially no effect on the peak value of $\sqrt{F}$ along either interface for this case. There is a significant difference in the interlaminar stresses in the tapered region ($0 \leqslant x/t_d \leqslant 4$), however these stresses are well below the peak values at the end of the dropped plies and are therefore not considered critical.

It is informative to examine the interlaminar stress components separately to determine their relative contributions to the delamination fraction. The distribution of σ_{nn} and σ_{tn} (σ_{yn} is approximately zero) along the upper interface are shown in Figs 6 and 7. (A value of $N_x = -1$ kN/m represents an average compressive σ_{xx} stress in the thin section of the laminate of 445 kPa.) The maximum value of the delamination fraction coincides with the maximum values of both the interlaminar normal and shear stresses, which also are not significantly influenced by eccentricity. This indicates that for this layup and loading, the

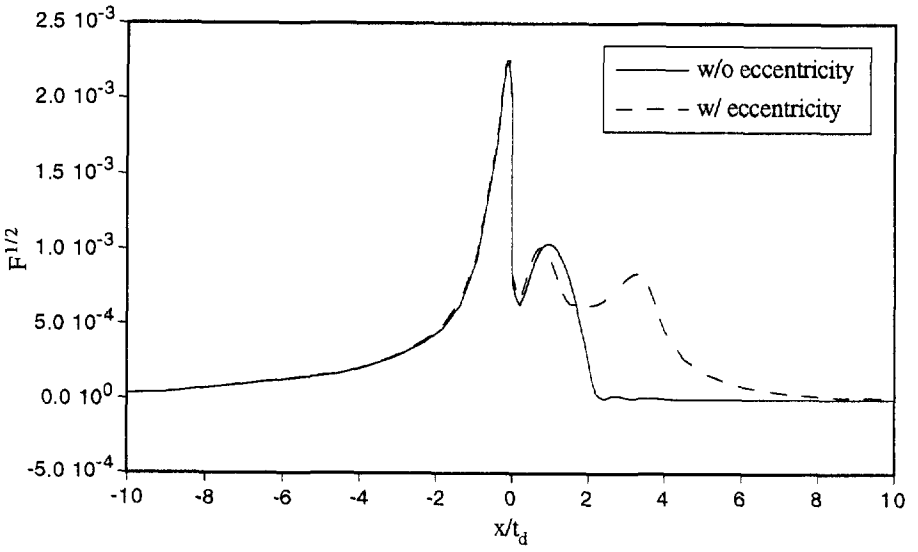

Fig. 5. Delamination fraction along the upper interface for four 0° plies dropped and the laminate loaded in longitudinal compression ($N_x = -1$ kN/m).

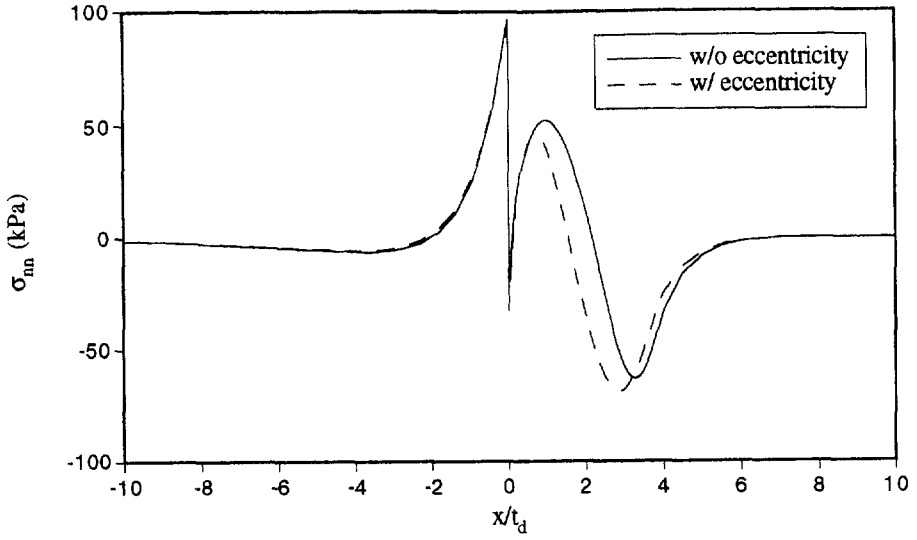

Fig. 6. σ_{nn} along the upper interface for four 0° plies dropped and the laminate loaded in longitudinal compression ($N_x = -1$ kN/m).

stiffness discontinuity influences the interlaminar stresses much more than the eccentricity. As for the relative contribution of the two stress components, the peak interlaminar normal tensile value of 97 kPa is 0.18% of Z^T while the peak interlaminar shear is -150 kPa, or 0.16% of Z^{S1}. This suggests that these components will have a comparable influence on the delamination of these laminates.

From the left end up to about $x = 2t_d$, the delamination fraction along the upper interface is very similar for the eccentric and centric geometries. Each has a maximum at $x = 0$ with a second peak at about $x = t_d$ (the plots of the interlaminar stresses show that this second peak is caused by a second peak in the tensile interlaminar normal stress). The delamination fraction is affected by the addition of eccentricity in the region $2t_d < x < 4t_d$, where an additional peak arises. As shown in Figs 6 and 7, this second peak is due to an increase in the interlaminar shear stress in that region. This shear peak is in turn due to a reversal in the bending moment through the transition region caused by the eccentricity, which introduces the additional negative shear. While this second peak in the delamination fraction is an interesting consequence of the presence of eccentricity, its magnitude is still

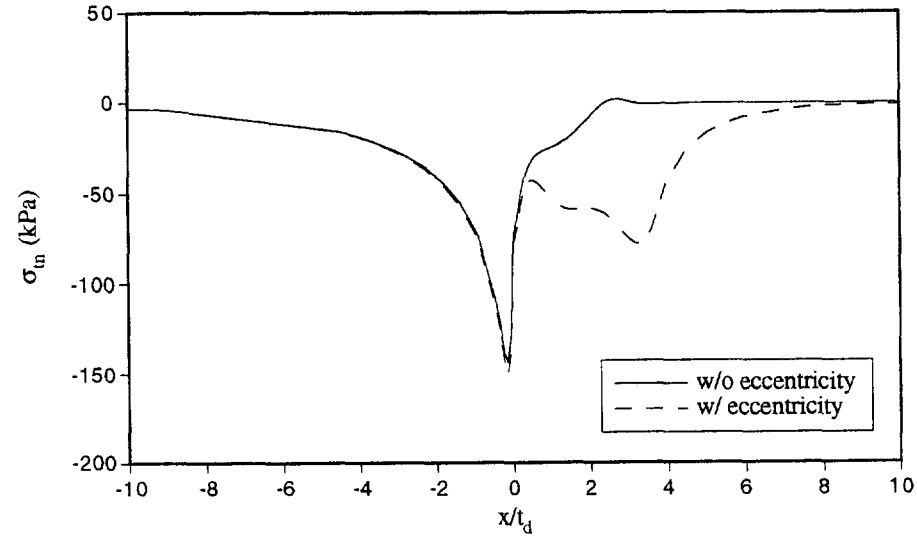

Fig. 7. σ_{tn} along the upper interface for four 0° plies dropped and the laminate loaded in longitudinal compression ($N_x = -1$ kN/m).

slightly less than the peak in the transition region that occurs without eccentricity and much less than the maximum that is located at the end of the dropped plies.

For the longitudinal compression loading, the $[90_4]_T$ dropped-ply layup experiences the largest change in the delamination fraction due to eccentricity, a 15% increase from 1.22×10^{-3} to 1.4×10^{-3}. However, experimental results presented by Curry *et al.* (1992) indicate that this configuration does not tend to fail by delamination under longitudinal compression. The fact that this layup has the smallest change in longitudinal stiffness and also the smallest values of $\sqrt{F}$ again indicates the larger role that the stiffness discontinuity plays in the delamination of dropped-ply laminates. The $[\pm 45]_s$ dropped-ply layup loaded in longitudinal compression only experiences an increase of 3% in $\sqrt{F}$ due to eccentricity.

The values of $\sqrt{F}$ for the transverse tension loading are all well below the values for the $[90_4]_T$ layup loaded in longitudinal compression, which again are below that required for a delamination failure at this level of load. Therefore, none of these three layups subjected to transverse tension would be expected to delaminate. The largest increase in $\sqrt{F}$ due to eccentricity for this loading is 11% for the $[90_4]_T$ layup.

The shear loaded case also has its largest increase in $\sqrt{F}$ due to eccentricity occurring for the $[90_4]_T$ drop. This is also the layup with the smallest value for the delamination fraction, again too small to induce a delamination failure. The $[\pm 45]_s$ dropped-ply layup, the stiffest with respect to shear, has the largest values of $\sqrt{F}$ for any of the cases examined, peaking at 3.65×10^{-3} for the eccentric geometry. However, this represents an increase of only 3% over the centric case.

Therefore, it appears that eccentricity does not significantly affect these laminates' capability to resist delamination initiation when loaded by longitudinal compression, transverse tension, or in-plane shear. This does not imply that these laminates will not delaminate, only that the presence of eccentricity of the middle surface does not appear to make this mode of failure significantly more likely than for laminates without eccentricity.

Stiffness discontinuity study

Clearly, the results of the study examining the effect of the eccentricity of the ply drop-off indicate that the stiffness discontinuity has a much greater influence on the magnitude of the interlaminar stresses than the eccentricity. Therefore, we examine the relationship between the stiffness of the dropped plies and the resulting interlaminar stresses.

The geometry of the laminate examined is the same as the eccentric dropped-ply laminate of the eccentricity study which is shown in Fig. 3(a). Four plies are dropped from between two eight ply quasi-isotropic $[\pm 45/0/90]_s$ sublaminates with the bottom surface of the laminate flat. The stiffness of the four dropped plies is varied by altering the angle θ in the balanced angle-ply layup $[\pm \theta]_s$. Five orientations for the angle θ are examined: 0°, 30°, 45°, 60°, and 90°. These layups are subjected to longitudinal compression and in-plane shear loadings for a total of ten different cases. The transverse tension loading examined in the eccentricity study is not repeated here because of the relatively low interlaminar stresses found for that loading.

The material properties used are again those of AS4/3502 graphite/epoxy. The dimensions of the laminate and the discretization used in modeling it are the same as those of the eccentricity study. The modeling of the $\theta = 90°$ case, however, does represent a change worth noting. In the eccentricity study, the 90° fibers were assumed to migrate into the region occupied by resin for the other orientations. The present study, being more interested in determining the effect of the magnitude of the stiffness discontinuity, uses the same location of the material discontinuity ($x = 0$) for $\theta = 90°$ as for the other layups and retains the triangular shaped resin region.

The distributions of the delamination fraction for the five different dropped-ply layups along the lower and upper interfaces for the longitudinal compression load case ($N_x = -1$ kN/m) are shown in Figs 8 and 9. Clearly, the peak value of the delamination fraction increases with increasing longitudinal stiffness of the dropped plies, as expected. In addition, the decay length into the thick section required for the induced interlaminar stresses to vanish also increases. The interlaminar stresses within the tapered region ($0 \leqslant x/t_d \leqslant 4$) do not vary significantly with the stiffness of the dropped plies.

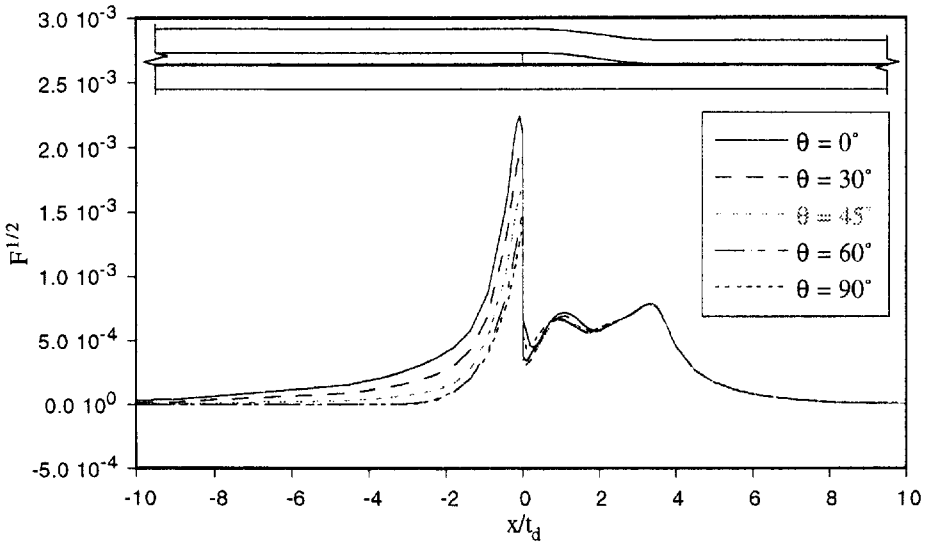

Fig. 8. Delamination fraction along the lower interface for different values of θ of the dropped sublaminate $[\pm\theta]_s$ ($N_x = -1$ kN/m).

Similar results are obtained for the in-plane shear loaded case shown in Figs 10 and 11 with the in-plane shear stiffness of the dropped plies as the major factor influencing the magnitude of $\sqrt{F}$. That is, the $\theta = 45°$ case has the largest peak in $\sqrt{F}$ as well as the greatest in-plane shear stiffness. As the value of θ increases or decreases from 45°, the in-plane shear stiffness of the dropped plies decreases as does the peak $\sqrt{F}$. An interesting difference between the response under in-plane shear and longitudinal compression loadings is that the decay length of the interlaminar stresses is shorter for the shear loading.

In work of Curry *et al.* (1992), a good experimental correlation was found between the ratio of the longitudinal stiffness of the thick to the thin sections of a dropped-ply laminate and the ratio of the compressive strength of the thin section to the compressive strength of the dropped-ply laminate (tested independently). Despite the fact that this correlation neglects the change in failure mode from that of the thin section (compressive strength failure) to that of the dropped-ply laminate (delamination), the agreement was very good. A similar approach is now taken in looking for correlation between the magnitude of the stiffness change and the interlaminar stresses introduced.

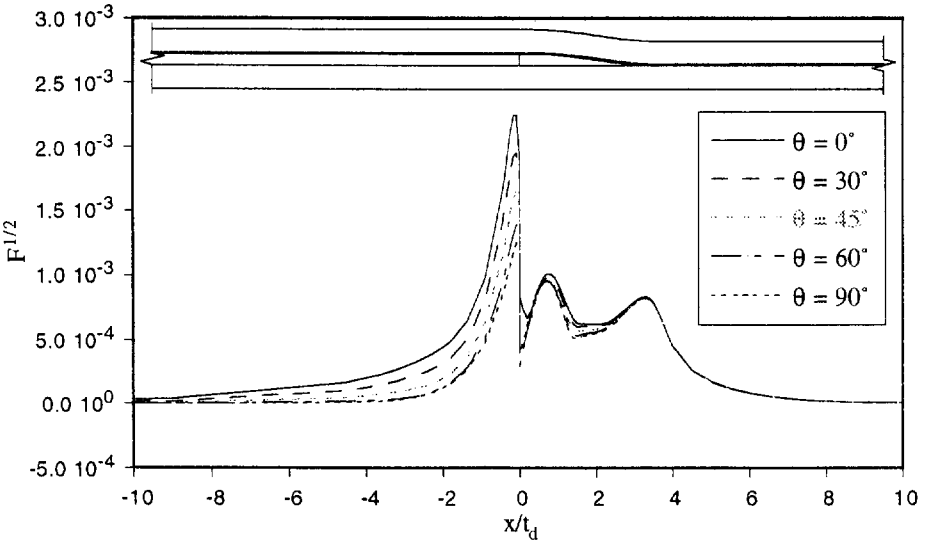

Fig. 9. Delamination fraction along the upper interface for different values of θ of the dropped sublaminate $[\pm\theta]_s$ ($N_x = -1$ kN/m).

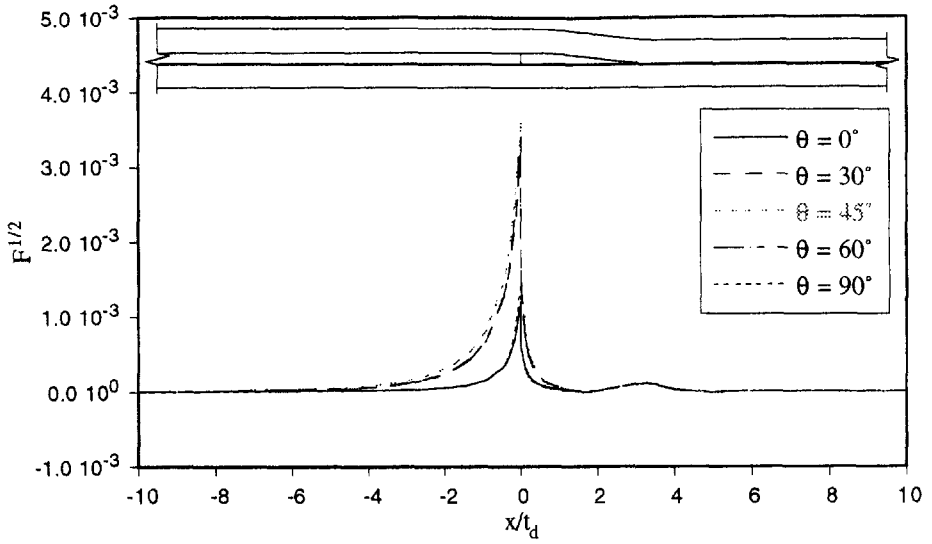

Fig. 10. Delamination fraction along the lower interface for different values of θ of the dropped sublaminate $[\pm\theta]_s$ (N_{xy} = 1 kN/m).

In Curry's examination of the effect of stiffness change, strain gage measurements were used to determine the average stiffness of the thick and thin sections of the laminate and a ratio of the two values was computed. The present study, being purely analytical, will rely on an estimation of this ratio based on classical lamination theory (CLT). Since the loading in the present study consists of an applied N_x with ε_y constrained to zero through the prescription of the out of plane deformations, the stiffness coefficient from CLT of interest is A_{11}. That is, this loading can be thought of as an applied strain field of $\varepsilon_x \neq 0$ with $\varepsilon_y = 0$. Because both symmetric angle-ply and quasi-isotropic laminates have zero shear-extension coupling terms A_{16} and A_{26}, no γ_{xy}° is induced and the applied N_x is related to ε_x° through the relation $N_x = A_{11}\varepsilon_x^{\circ}$ in CLT.

Rather than correlating the stiffness change to a measured failure load as did Curry *et al.*, the present study will use the peak value of the delamination fraction. The values of the longitudinal stiffness ratio for the five dropped-ply laminates examined are plotted vs the

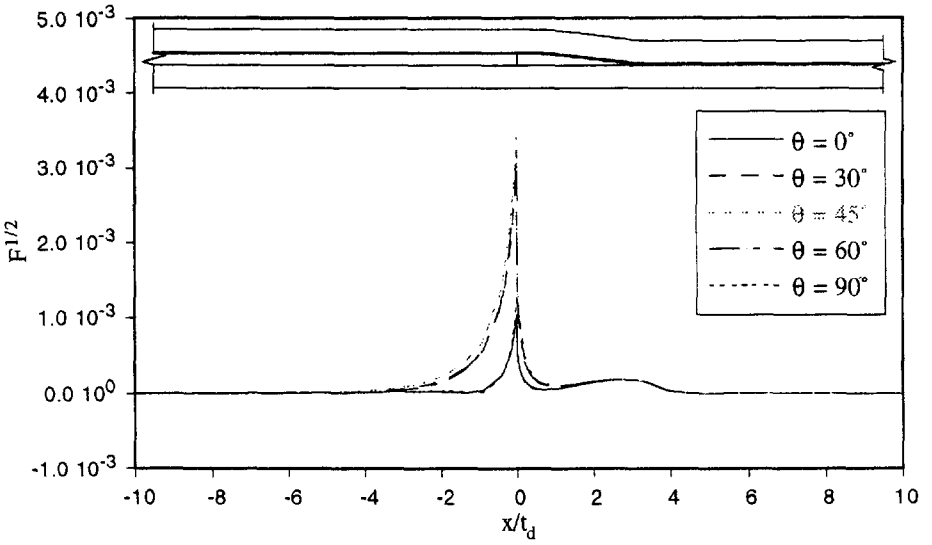

Fig. 11. Delamination fraction along the upper interface for different values of θ of the dropped sublaminate $[\pm\theta]_s$ (N_{xy} = 1 kN/m).

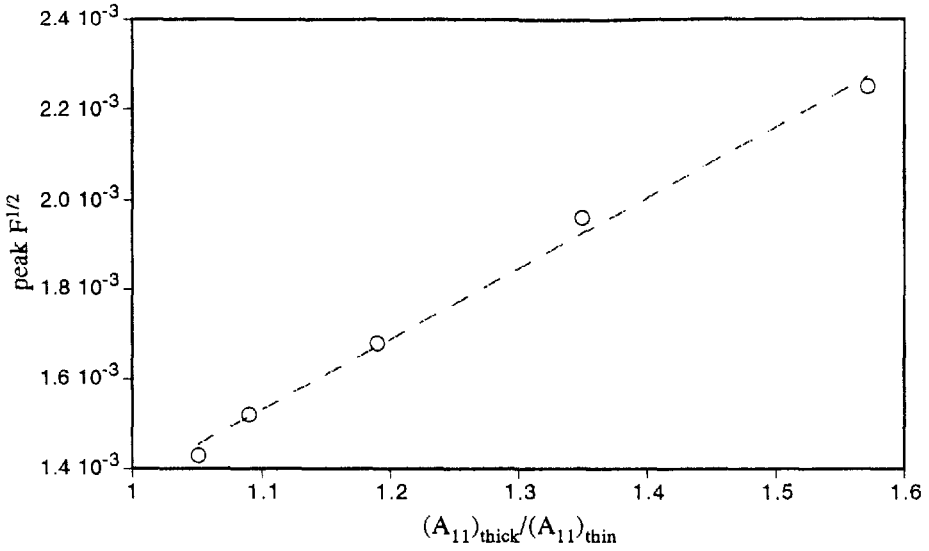

Fig. 12. Plot of the correlation between the stiffness ratio and the peak value of $\sqrt{F}$ (longitudinal compression loading).

peak $\sqrt{F}$ values in Fig. 12 along with a linear least squares fit. Although not compared to a baseline case of a uniform thickness specimen (as did Curry *et al.*) since this would correspond to a zero value of $\sqrt{F}$, these results indicate that if failure is based on the magnitude of the peak value of $\sqrt{F}$, an increase in the longitudinal stiffness ratio will result in a proportional decrease in failure load of the dropped-ply laminate.

A similar examination of the in-plane shear loaded cases can be made by using the A_{66} stiffness coefficient instead of A_{11}. This choice is easily justified by the aforementioned decoupling of the shear and extension for balanced, symmetric angle-ply and quasi-isotropic laminates. A plot of a linear least squares fit of the ratios in A_{66} vs the peak values of $\sqrt{F}$ is shown in Fig. 13. While the correlation here is not as good as for the longitudinal compression case, the trend is clearly represented. This is a somewhat curious result because, unlike the longitudinal compression case, which has significant contribution from both σ_{nn} and σ_{tn}, the value of $\sqrt{F}$ for the in-plane shear loading is entirely due to one stress component, the out-of-plane interlaminar shear stress σ_{yn}. The most obvious deficiency here

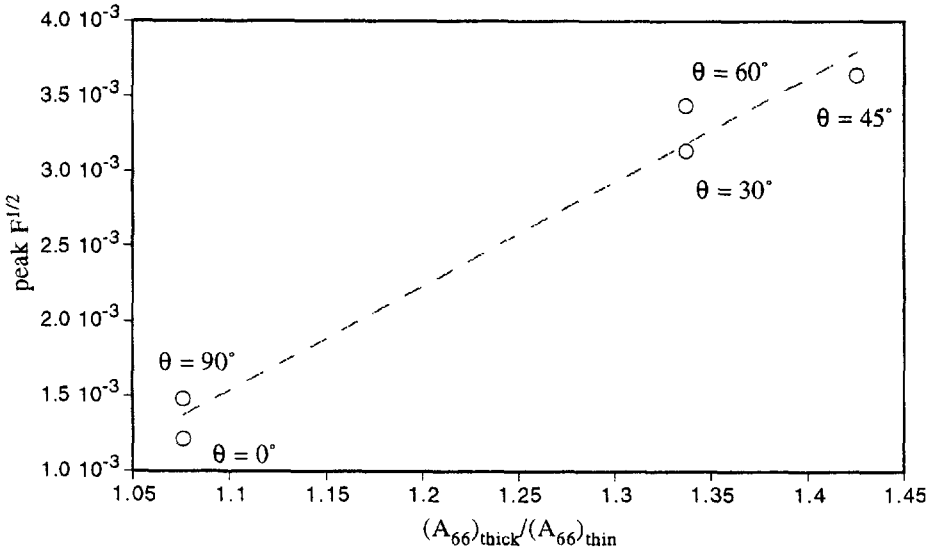

Fig. 13. Plot of the correlation between the stiffness ratio and the peak value of $\sqrt{F}$ (in-plane shear loading).

lies in the fact that A_{66} is symmetric with respect to θ about 45° for these layups while the peak values of $\sqrt{F}$ are not. The cause of this lack of symmetry lies in the difference in transverse shear stiffnesses G_{13} and G_{23} for a unidirectional ply, which do not enter into CLT. Because of the generalized plane deformation assumption of the present theory, the shear strain produced by the applied shear loading is due entirely to $\partial v/\partial x$, as $\partial u/\partial y$ is zero. As a consequence, the load is transferred to the dropped plies only through σ_{yn} as mentioned above. Therefore, a ply oriented such that it has a greater shear stiffness in the y-z plane will have larger interlaminar stresses for this shear loading. This would correspond to a θ closer to 90° rather than 0° and indeed these are the layups with the larger value of $\sqrt{F}$ in Fig. 13.

This difference in transverse shear stiffnesses G_{13} and G_{23} also affects the load transfer for the longitudinal compression loading, however, in that case both σ_{nn} and σ_{tn} are major contributors to the peak value of the delamination fraction. Thus, the influence of the transverse shear stiffnesses G_{13} and G_{23} on the delamination fraction in longitudinal compression is not as important as it is in the shear loading case.

A few other points regarding these correlations are worth noting. First, the fact that neither linear least squares fits pass through $\sqrt{F} = 0$ for a stiffness ratio of 1.0 indicates that other influences are contributing to the value of $\sqrt{F}$. These other influences are the geometry of the taper and the presence of the material discontinuity, neither of which need be accompanied by a stiffness change. For example, a laminate with the same taper geometry could be made with the dropped plies replaced by resin, leaving a laminate with a ratio of CLT stiffnesses of approximately one. A material discontinuity also need not be accompanied by a stiffness change as defined here. Wisnom's (1991, 1992) work examining laminates with cut, but not discontinued, internal plies is an example of such a configuration. Wisnom found this to be the greatest single factor contributing to delamination of unidirectional laminates containing dropped plies loaded longitudinally.

CONCLUDING REMARKS

A mixed variational formulation for the generalized plane deformation response of laminated plates that taper abruptly in thickness is developed, with particular emphasis on interlaminar stress prediction. Both interlaminar displacement and traction continuity are imposed on the model developed, and are satisfied point-wise in the interface. The formulation is a modification of Pagano's (1978, 1983) theory in which the stress field is assumed explicitly in the thickness coordinate and the Hellinger-Reissner variational principle is employed. Modifications include the development of the shape functions used in the assumed stress field as well as the displacement weighting functions used in integrating the principle through the thickness. The changes to the weighting functions corrected numerical difficulties encountered when attempting to directly apply Pagano's approach to laminates with thin layers relative to other layers or with thin layers a large distance from the reference plane.

The approach for the solution of the governing equations was also changed. Manipulation of the governing equations, which form a differential-algebraic system, to give an equal number of differential equations and boundary conditions clarifies the selection of end conditions. The algebraic equations were then differentiated and imposed in their original form as initial conditions in order to allow for conventional two point boundary value problem solution methods. The resulting set of equations was solved by a higher order (two stage Gauss implicit Runge-Kutta) one step finite difference scheme. Pagano *et al.* (1985, 1986) used central, forward, and backward finite differences to solve a system of equations which were developed assuming the integrand in the functional vanished at the end points.

These changes combined to allow the straightforward application to the analysis of dropped-ply laminates which included modeled resin layers less than 5% the thickness of a single ply.

Parametric studies of laminates of varying dropped-ply sublaminate layups under different loading conditions showed that the stiffness of the dropped plies has a much larger

influence on the interlaminar stresses produced than does the eccentricity of the load path through the thickness discontinuity. In addition, a good correlation was found between the ratio of stiffnesses between the thick and the thin sections and the peak value of the delamination fraction, $\sqrt{F}$.

Acknowledgment—This research was supported by the NASA Langley Research Center under grant NAG1-343, the NASA-Virginia Tech Composites Program.

REFERENCES

Ascher, U. M., Mattheij, R. M. M. and Russell, R. D. (1988). *Numerical Solution of Boundary Value Problems for Ordinary Differential Equations*, pp. 210–216, Prentice Hall.

Barlow, J. (1976). Optimal stress locations in finite element models. *Int. J. Num. Meth. Engng* **10,** 243–251.

Brewer, J. C. and Lagace, P. A. (1988). Quadratic stress criterion for initiation of delamination. *J. Comp. Materials* **22,** 1141–1155.

Curry, J. M., Johnson, E. R. and Starnes, Jr, J. H. (1992). Effect of dropped plies on the strength of graphite-epoxy laminates. *AIAA J.* **30,** 449–456.

Fish, J. C. and Lee, S. W. (1989). Delamination of tapered composite structures. *Engng Fract. Mech.* **34,** 43–54.

Harrison, P. N. and Johnson, E. R. (1993). A mixed formulation for interlaminar stresses in dropped-ply laminates. In *Proc. 34th AIAA/ASME/ASCE/AHS/ASC Structures, Structural Dynamics, and Materials Conference*, La Jolla, CA, AIAA Paper 93-1508-CP, pp. 1740–1752. AIAA, Washington, DC.

Harrison, P. N. (1994). Interlaminar stress analysis of dropped-ply laminated plates and shells by a mixed method. Doctoral Dissertation, pp. 144–152. Aerospace Engineering. Virginia Polytechnic Institute and State University, Blacksburg, VA.

Lekhnitskii, S. G. (1981). *Theory of Elasticity of an Anisotropic Body*, English translation, p. 122. Mir Publishers, Moscow.

Pagano, N. J. (1978). Stress fields in composite laminates. *Int. J. Solids Structures* **14,** 385–400.

Pagano, N. J. (1983). Axisymmetric stress fields in involute bodies of revolution. In *Advances in Aerospace Structures, Materials and Dynamics; A Symposium on Composites, AD-06*, Boston, MA (Edited by U. Yuceoglu, R. L. Sierakowski and D. A. Glasgow), pp. 57–64. American Society of Mechanical Engineers, New York, NY.

Pagano, N. J. and Whitford, L. E. (1985). On the solution for the elastic response of involute bodies. *Comp. Sci. and Tech.* **22,** 295–317.

Pagano, N. J. (1986). Refined solutions for the elastic response of involute bodies. *Comp. Sci. and Tech.* **25,** 251–270.

Salpekar, S. A., Raju, I. S. and O'Brien, T. K. (1988). Strain energy release rate analysis of delamination in a tapered laminate subjected to tension load. In *Proc. American Society for Composites Third Technical Conference*, Seattle, WA, pp. 642–654.

Sandhu, R. S., Wolfe, W. E. and Chyou, H. H. (1991). Variational formulation and finite element implementation of Pagano's theory of laminated plates. Final report to air force systems command. *WL-TR*-91-3016, *NASA* # *N*92-29594, Dept of Civil Engineering, The Ohio State University.

Schiesser, W. E. (1994). *Computational Mathematics in Engineering and Applied Science: ODEs, DAEs, and PDEs*, pp. 7–8 CRC Press Inc., Boca Raton, FL.

Wisnom, M. R. (1991). Delamination in tapered unidirectional glass fibre-epoxy under static tension loading. In *Proc. 32nd AIAA/ASME/ASCE/AHS/ASC Structures, Structural Dynamics and Materials Conference*, Baltimore, MD, AIAA Paper No. 91-1142-CP, pp. 1162–1172. AIAA, Washingon, DC.

Wisnom, M. R. (1992). Prediction of delamination in tapered unidirectional glass fibre epoxy with dropped plies under static tension and compression. In *AGARD CP*530, *Specialists Meeting on Debonding/Delamination of Composites*, Patras, Greece, 25-1–25-7.